Nat. Hazards Earth Syst. Sci. Discuss., 1, 2831–2857, 2013
www.nat-hazards-earth-syst-sci-discuss.net/1/2831/2013/
doi:10.5194/nhessd-1-2831-2013

Natural Hazards and Earth System Sciences
Open Access
Discussions

Modelling of tsunami wave run-up, breaking and impact on vertical wall by SPH method

M. H. Dao[1], H. Xu[2], E. S. Chan[3], and P. Tkalich[2]

[1]Center for Environmental Sensing and Modeling, Singapore-MIT Alliance for Research and Technology, Singapore
[2]Tropical Marine Science Institute, National University of Singapore, Singapore
[3]Department of Civil Engineering, National University of Singapore, Singapore

Received: 21 May 2013 – Accepted: 3 June 2013 – Published: 22 June 2013

Correspondence to: M. H. Dao (myha@smart.mit.edu)

Published by Copernicus Publications on behalf of the European Geosciences Union.

Abstract

Accurate predictions of wave run-up and run-down are important for coastal impact assessment of relatively long waves such as tsunami or storm waves. Wave run-up is, however, a complex process involving nonlinear build-up of the wave front, intensive wave breaking and strong turbulent flow, making the numerical approximation challenging. Recent advanced modeling methodologies could help to overcome these numerical challenges. For a demonstration, we study run-up of non-breaking and breaking solitary waves on vertical wall using two methods, the enhanced Smoothed Particle Hydrodynamics (SPH) method and the traditional non-breaking nonlinear model Tunami-N2. The Tunami-N2 model fails to capture the evolution of steep waves at the proximity of breaking that observed in the experiments. Whereas, the SPH method successfully simulate the wave propagation, breaking, impact on structure and the reform and breaking processes of wave run-down. The study also indicates that inadequate approximation of the wave breaking could lead to significant under-predictions of wave height and impact pressure on structures. The SPH model shows potential applications for accurate impact assessments of wave run-up onto coastal structures.

1 Introduction

The recent tsunami generated by the Honshu Earthquake in 2011 caused tremendous damages to residential and industrial installations at the affected area. Approximately 15 000 people were killed and more than 300 000 buildings were damaged by the earthquake and tsunami (Mimura et al., 2011). The deep-inland and powerful run-up of the tsunami wave has damaged the power cooling units of the Fukushima nuclear power plant, triggered one of the world scariest nuclear disaster (US Geological Survey, 2012). All of these and with the lessons learnt from the 2004 Indian Ocean Tsunami disaster have shown that in spite of studies during past decades, the run-up threats and destructive forces of those powerful waves have still been underestimated.

NHESSD

1, 2831–2857, 2013

Various numerical methods have been developed to predict the tsunami wave run-up. Because of hydrodynamic similarities, researchers often use solitary waves as initial conditions to investigate the tsunami run-up characteristics. One of the most popular methods is the Boundary Integral Method (BIM) for potential flow. Although BIM can get accurate free surface of non-breaking waves (Kim et al., 1983; Maiti and Sen, 1999), the method is very limited when simulating the wave breaking of steep wave fronts (Dommermuth et al., 1988; Grilli et al., 1997). The Eulerian Nonlinear Shallow Water Equation (ENSWE) solvers have been used to simulate long wave propagation and run-up (Li and Raichlen, 2003; Liu et al., 1995; Titov and Synolakis, 1998; Tkalich and Dao, 2011). The inherent numerical diffusion and dispersion, otherwise available in Boussinesq approximation, are often used to mimic the physical ones while a turbulence closure model is used to approximate sub-grid flows. The ENSWE method could simulate accurately the wave propagation and adequately the wave run-up. However, the method itself could not resolve the build-up and breaking of steep wave fronts without special treatments of the free surface. The ENSWE solvers coupled with free surface tracking methods, such as in Volume of Fluid or Level Set methods, have been successful in capturing the build-up and breaking of steep wave fronts. However, for very steep surface deformation and intensive breaking, very fine meshes are needed to resolve the breaking free surface and water jets created by the breaking wave fronts. Even thought, the mass conservation is still a challenge for the surface tracking methods, leading to inaccurate modeling of post-breaking processes.

Recently, meshless methods have become popular in modelling similar fluid dynamics problems. The Smooth Particle Hydrodynamics (SPH) is one of the most robust, efficient, stable and accurate meshless methods. The SPH method was first introduced independently by Gingold and Monaghan (1977) and Lucy (1977) and has later been modified for modelling wave breaking on beaches in two and three dimensions, green waters and wave structure interactions (Colagrossi and Landrini, 2003; Dalrymple and Rogers, 2006; Gomez-Gesteira et al., 2005). Dao (2010) and Dao et al. (2011) extended the method and simulated the propagation, focusing and breaking of a wave

NHESSD
1, 2831–2857, 2013

group in deep water using an advanced modeling methodology and a very fine resolution. Very promising results that have not been picked up in past numerical studies were obtained, including the wave front evolution, fine flow structures under breaking wave, water jets and sprays above the wave crest and the evolution of entrapped air bubbles. These features are very well matching with experimental observations.

The original SPH methods, although satisfying the mass conservation, still have zero order in the kernel approximation which sometimes leads to significant dissipation of momentum (Liu and Liu, 2006). Several studies (Bonet and Kulasegaram, 2000; Vidal et al., 2007; Oger et al., 2007) have introduced correction terms on the governing equations to improve the kernel approximation to first order. Xu et al. (2010) and Xu (2013) extended and implemented an enhanced correction method proposed by Liu and Liu (2006). The enhanced SPH model was used to simulate sloshing and solitary wave propagations and impacts onto structures. Obtained results showed significant improvement of momentum conservation. The enhanced SPH method is able to simulate wave propagations over a long distance, breaking and impact pressures at a satisfactory level of accuracy.

In this study, the enhanced SPH method is used to simulate solitary waves run-up, run-down over a sloping beach with breaking and impact on a vertical wall. The simulation results of the SPH model are compared with that of the famous tsunami model, Tunami-N2 (Goto et al., 1997), and verified against the experiments conducted at the US Army Engineer Waterways Experiment Station, Vicksburg, Mississippi (Ward, 1995). In the experiment, three types of solitary wave run-up, which include non-breaking, closed to breaking, and breaking wave, were considered. Brief introduction of important features of the numerical models are presented, whereas for more details, readers are referred to previous publications for SPH (Dao, 2010; Dao et al., 2010; Xu et al., 2010; Xu, 2013) and Tunami-N2 model (Goto et al., 1997; Dao and Tkalich, 2007).

NHESSD
1, 2831–2857, 2013

2 Numerical models

2.1 Governing equations

The wave propagation and run-up can be governed by the Navier–Stokes equations which takes the form of

$$\frac{\mathrm{d}\rho}{\mathrm{d}t} = -\rho\nabla\cdot\boldsymbol{u} \tag{1}$$

$$\frac{\mathrm{d}\boldsymbol{u}}{\mathrm{d}t} = -\frac{1}{\rho}\nabla p + \boldsymbol{g} \tag{2}$$

where, ρ and p are the density and pressure of the fluid; In two-dimensional space, $\boldsymbol{u} = (u_x, u_y)$ is the fluid velocity and $\boldsymbol{g} = (g_x, g_y)$ is the gravitational acceleration.

2.2 SPH model

SPH method uses a set of discrete particles to approximate the fluid domain. The governing equations are approximated by the interaction of particles within a support domain of a kernel function. This approximation allows the divergences and gradients of fluid properties are transferred to the kernel function. The formulas take the following forms:

$$\frac{\mathrm{d}\rho_i}{\mathrm{d}t} = -\rho_i\nabla\cdot\boldsymbol{u} = -\rho_i\sum_j \frac{m_j}{\rho_j}\left(\boldsymbol{u}_j - \boldsymbol{u}_i\right)\cdot\nabla_i W_{\mathrm{ij}} \tag{3}$$

$$\frac{\mathrm{d}\boldsymbol{u}_i}{\mathrm{d}t} = -\sum_j m_j\left(\frac{p_i}{\rho_i\rho_j} + \frac{p_j}{\rho_i\rho_j}\right)\nabla_i W_{\mathrm{ij}} + \boldsymbol{g}_i \tag{4}$$

$$\frac{\mathrm{d}\boldsymbol{x}_i}{\mathrm{d}t} = \boldsymbol{u}_i \tag{5}$$

where i and j are the particle indices, m is the mass of the particles, $\boldsymbol{x}$ is the position of the particles, and W is the kernel function. In this study, the following 5th order Quintic

NHESSD
1, 2831–2857, 2013

kernel function is used:

$$W_{ij} = W(q) = \alpha_D \left(1 - \frac{q}{2}\right)^4 (2q+1)\,, \quad 0 \le q \le 2 \tag{6}$$

where, $\alpha_D = 7/(4\pi h^2)$ and $q = \| \boldsymbol{x} - \boldsymbol{x}' \| / h$ is the normalized distance from particle j to particle i. The parameter h, often called smoothing length, is a measure of the length scale of the support domain of the kernel function.

The relationship of the pressure and density of a particle follows the equation of state (Batchelor, 1967)

$$p_i(\rho) = \frac{\rho_o c_0^2}{\gamma} \left[\left(\frac{\rho_i}{\rho_o} \right)^{\gamma} - 1 \right] + p_o \tag{7}$$

where c_0 is the numerical sound speed, p_o is the reference pressure, ρ_o is the reference density and $\gamma = 7$ for water. This formulation allows particle density to change within a range controlled by the numerical sound speed, thus the approximated fluid is weakly compressible.

Simulations of wave generation, propagation, breaking and impact on structures by SPH have been verified in the previous studies by the authors (Dao, 2010; Dao et al., 2010; Xu et al., 2010; Xu, 2013).

2.3 Tunami-N2 model

The model Tunami-N2 used in this paper was originally developed in Disaster Control Research Center (Tohoku University, Japan) through the Tsunami Inundation Modeling Exchange (TIME) Program (Goto et al., 1997). Tsunami-N2 solves a set of nonlinear shallow water approximation of the Navier–Stokes equations. The model uses second-order explicit leap-frog finite difference scheme to discretize the set of nonlinear shallow water equations. Horizontal eddy turbulence is neglected and the bottom friction is computed from Manning formulation. No specific treatment of breaking surface was introduced in the model.

NHESSD
1, 2831–2857, 2013

Tunami-N2 model has been intensively verified using analytical solutions, laboratory experiments and real cases, and subsequently applied to simulate tsunami propagation and run-up in Pacific, Atlantic and Indian Oceans, with zoom-in at particular regional seas and coastal areas (Shuto et al., 1990; Shuto and Goto, 1988; Yalciner et al., 2004; Dao and Tkalich, 2007; Dao et al., 2008).

3 Solitary wave run-up simulations and discussions

3.1 Experiment setup

The experiment was conducted at the US Army Engineer Waterways Experiment Station, Vicksburg, Mississippi by Ward (1995). The wave flume consisted of a wave maker located at the left side of the flume, a flat bottom followed by three slopes (1 : 53, 1 : 150 and 1 : 13) and a vertical wall located at the right side (see Fig. 1). Still water depth at the flat section was $d = 21.8$ cm. Several wave gages were distributed in the flume to measure the surface elevation.

In the experiment, three different solitary waves were generated by the movement of the piston paddle. The target wave height, h_{tar}/d, of each case were 0.05 (case A), 0.3 (case B) and 0.7 (case C), respectively.

3.2 Numerical setups and calibrations

The same wave flume configuration as in the experiment is used in the SPH simulations. A total of about 1.1 million water particles of uniform diameter of $dx = 0.002$ m is used. The solitary waves are generated by moving the piston paddle in the model in the same ways as the experiment did. Because the time resolution of piston paddle recorded in the experiment is not at high resolution to derive an accurate paddle velocity, we use wave maker theory (Hughes, 1993; Khayyer et al., 2008) to improve the time history of paddle position and velocity. We observed that the paddle strokes computed by the theory are slightly larger than that measured in the experiment. Therefore, in

NHESSD
1, 2831–2857, 2013

order to generate comparable solitary waves, the computed paddle trajectories by the wave maker theory are scaled down to fit the experiment paddle strokes. The paddle velocities are also scaled down with the same ratio (see Fig. 2).

Each solitary wave generated in the SPH model is calibrated against measurements at gage 4 (see Fig. 3). In Case B, the numerical result matches well with the experiment. Case A shows a little over shoot while under prediction is seen in Case C. When comparing to the target wave height set in the experiment, h_{tar}/d, numerical result of Case A reads $h_{meas}/d = 0.0484$ while the experimental result is $h_{meas}/d = 0.0378$. The simulated wave height is closer to the target value of 0.05 for case A. In Case B, both numerical and experimental results read $h_{meas}/d = 0.251$, which is significantly different from the target value of 0.3. In case C, the numerical result is $h_{meas}/d = 0.594$ while the experimental result is 0.688. The experimental result is closer to the target value of 0.7. As sensitivity studies of the SPH model showed some expected gain of wave height in the simulation outputs when the wave propagates further, we keep these settings for further simulations and investigations of wave heights recorded at the downstream wave gages.

In the simulations by Tunami-N2, the numerical domain is similar to the real wave flume, except that the left boundary is truncated at the location of gage 4. The time histories of wave height recorded at gage 4 in the experiments are used as prescribed water elevation boundary condition at the left boundary. The horizontal resolution of $dx = 0.002$ m, which is equal to the particle size in the SPH simulations, is used in all simulations. Manning coefficient is 0.0025. No special treatment for wave breaking is added in Tunami-N2.

3.3 Numerical simulations of case A

In Case A the solitary wave propagates and run-ups on the slopes without breaking. In both numerical simulations and the experiment, the wave propagates towards the vertical wall and reflected by the vertical wall without prior breaking (see Fig. 4). The maximum wave heights of about two times of that at gage 4 (or about 0.1 times of still

NHESSD
1, 2831–2857, 2013

water depth) are observed in the simulation results. The waves are reflected by the vertical wall and no breaking happens during the impact.

Comparisons of wave height time histories at gages 5–10 extracted from numerical simulations and experiment are shown in Fig. 5. The wave heights obtained by Tunami-N2 match well with the experiment records at all gages while that of the SPH simulation are slightly higher. When the wave approaches to the toe of the second slope (gage 5), wave height obtained by the SPH simulation increases about 10 % from that at gage 4. Incident wave height of 0.02 m is observed at gage 10 in the SPH simulation. The reflected wave is captured in both numerical simulations (the second peaks shown in Fig. 5). Again, the reflected wave in Tunami-N2 is closer to the experiment result than the SPH result. In overall, Tunami-N2 achieves better result than SPH in comparison with experiment. However, one must note that the incident wave at gage 4 used the Tunami-N2 takes the exact value of the experiment, while that of SPH is generated by numerical wave paddle and are slightly different from the experiment record.

3.4 Numerical simulation of case B

In case B, the incident wave in the experiment is steep and breaking possibly takes place. Snapshots of the solitary wave approaching and impacting on the vertical wall obtained from the SPH simulation are shown in Fig. 6. Comparisons of time histories of wave height at gages 5–10 obtained from numerical simulations and experiment are shown in Fig. 7. Incident wave from both SPH and Tunami-N2 simulations agree well with experiment results at gage 5 and gage 6. At gage 7, both numerical incident waves are lower than that in the experiment. The SPH result is closer to the experiment than that of the Tunami-N2. At gage 8 and gage 9, the SPH result agrees very well with experiment while the Tunami-N2 wave height decreases drastically. We can see in Fig. 7 that, the wave is already very steep when it is passing by gage 7. High nonlinearity evolution of the wave front is captured in the SPH but not in the Tunami-N2. That could attribute to the sharp reduction of wave height in the Tunami-N2 simulation. At gage 10, wave height recorded in the experiment decreases remarkably while that of the SPH

NHESSD
1, 2831–2857, 2013

simulation does not. It may be because the wave breaking may occur in the experiment somewhere in between gage 9 and gage 10 but not occur in the simulation. As we could see from the simulation results in Fig. 6, when the wave approaches the wall the wave front is steepening but no breaking is observed (Fig. 6a, b). Incident wave height of 0.09 m is observed at this gage in the SPH simulation. The wave directly impacts on the wall creating a water jet shooting upwards that can reach more than three times of the still water depth (Fig. 6c).

The SPH simulation also captures well the reflected wave (the second peak in the time series). At gage 10, the reflected wave recorded in the experiment is significantly lower than that in the SPH simulation. It could be because the incident wave in experiment already broke before hitting the wall (as discussed above). The experimental and SPH time histories at gage 9 show that the reflected wave could be steepened and break again. The reflected wave in Tunami-N2 is significantly lower than that in the experiment. Overall, the SPH performs much better than Tunami-N2 in Case B where wave is very steep and breaking possibly takes place.

3.5 Numerical simulation of case C

In case C, the incident wave is definitely broken before impacting on the wall. The wave breaking is captured in the SPH simulation as shown in Fig. 8. As wave propagates over the slope, the wave steepness increases. The wave front becomes very steep and a jet is generated in front of the wave and is projecting forward (Fig. 8a). The jet curls over and plunges onto the water surface in front generating a process called wave breaking (Fig. 8b–h). Details of the wave breaking process are out of the scope of this paper. Interested readers could refer to Dao (2010) for the discussions on wave breaking.

Comparisons of time histories of wave height recorded at gages 5–10 obtained from the numerical simulations and experiment are shown in Fig. 9. At gage 5, both numerical results of incident wave agree well with the experiment. The wave steepens when passing by gage 6 and 7. The SPH simulation captures very well the steepening process while the Tunami-N2 does not. The incident wave heights recorded at these gages

NHESSD
1, 2831–2857, 2013

from the SPH simulation match well the experimental data, while the Tunami-N2 shows a sudden drop in wave height after gage 5 due to lack of the wave breaking modelling capability. The reduction of wave height could be a result of large numerical dissipation in the simulation when the gradient of the free surface is very large. Wave steepening sometimes causes Tunami-N2 blow-up if the time stepping is not small enough. Spurious oscillations may appear at the rear of the wave when it is too steep as seen at gage 5 and gage 6.

Figure 9 indicates that wave breaking happens somewhere in between gage 7 and gage 8 as sharp drops in wave heights are observed in both SPH and experiment results. Very good agreements are also observed between SPH and experiment results at gage 9 and gage 10, including the reflected wave (the second peak in the time series). Incident wave height of 0.08 m is observed at gage 10 in the SPH simulation. There are differences between SPH and experiment results observed, however, it is difficult to quantify because the breaking wave causes significant difficulties in measuring water level in both numerical simulation and experiment. Tunami-N2 consistently under-predicts both the incident and reflected waves. Moreover, due to the predicted lower total water depth, the wave travels slower and arrives later in the Tunami-N2 simulation as compared to that in the experiment and SPH simulation. In overall, Tunami-N2 performs very badly as compared with SPH in Case C where wave breaking takes place early.

Snapshots of breaking wave impact on the vertical wall simulated by SPH are shown in Fig. 10. The solitary wave breaks at the second slope from the left and continues to propagate forward to the wall on the right. The wave front is composed by water sprays splashing forwards instead of a sharp interface (Fig. 10a). The splash of water is approaching the wall (Fig. 10b). As the whole breaking wave hits the wall, water splashes upward and the water elevation at the wall increases quickly (Fig. 10c). The main part of the reformed wave impacts on the wall and creates an upward water jet. Water surface at the wall continues to rise and the water jet shoots up. The water jet could reach up to 2.5 times of the still water depth (Fig. 10d) before falling down and

NHESSD
1, 2831–2857, 2013

impact on the water surface near the corner (Fig. 10e). Even though the incident wave is almost double that of Case B, the ratio of maximum run-up height over the still water depth is lower. This could be attributed to the large amount of wave energy dissipated through the breaking before the wave hits the wall.

3.6 Impact pressure on wall

Wave impacts on marine and coastal structures have been studied intensively in the past. Experimental studies have shown that the peak pressures due to wave impact could be more than 10 times of that generated by waves of similar amplitude but without impact and the magnitude of peak pressure is primarily determined by the stage of wave breaking prior to wave impact (Chan and Melville, 1988; Chan, 1994; Chan et al., 1995). A recent study by Lugni et al. (2006) showed that a flip-through wave impact (without prior breaking) on a vertical wall could generate a pressure of 3 to 6 times of a non-impact wave run-up at the impact area. Impact pressures of breaking wave onto vertical wall have been successfully modelled by the SPH program developed by the authors. The SPH was able to pick up accurately the magnitudes of the impact pressures and shapes of pressure evolutions observed in Lugni et al. (2006) experiments (Xu, 2013).

In the SPH simulations of the solitary waves in this study, the numerical pressure sensor is located on the wall at the initial still water level. The recorded pressure is normalized to the hydrostatic pressure increase due to incident wave at the nearest gage (gage 10), $\rho g h_{10}$. Results of the three cases are shown in Fig. 11. When the wave hits the wall and reflects, the pressure measured in Case A shows a gradual increase then decrease. The peak pressure is approximately $1.2\rho g h_{10}$. This is, indeed, mostly contributed by the increase of static pressure which is characterized by the increase and decrease of water level at the wall. In Case B and Case C, sharp rises of pressures followed by pressure oscillations are observed. Case B characterizes a typical flip-through wave impact. The peak pressure in this case is approximately $3.2\rho g h_{10}$. The

NHESSD
1, 2831–2857, 2013

impact pressure of Case C even reaches $7.4\rho g h_{10}$. Numerical results of Case B and C are consistent with that observed in the experiments of wave breaking and impact referred above.

4 Conclusions

In this study, three cases of solitary wave propagation and run-up were simulated by the SPH and the Eulerian Nonlinear Shallow Water (Tunami-N2) numerical models. Comparisons of the simulated wave height time series with the experiments showed that Tunami-N2 is only suitable for non-breaking waves, where as the SPH method showed the full capability to simulate the whole process of a wave run-up, including complex wave breaking and tremendous impact pressure. The study also highlighted that neglecting or inadequate numerical scheme for the approximation of breaking waves could lead to significant under-predictions of run-up height and impact pressure on coastal structures.

The SPH method is much more computationally intensive than the ENSWE. The computational demanding sometimes prohibits the SPH method from real-time applications. However, the method is very useful in post studies of extreme events or in designing structures that subject to complex wave impact. It is also useful in constructions of wave run-up database in which combinations of different beach slopes and incident waves are simulated off-line. Such databases will be used for data-mining or data-driven models that could provide quick and adequate impact assessments of tsunami or storm waves run-up on beaches given the incident waves obtained from a real-time ENSWE model.

Acknowledgements. The research described in this publication was supported by the Singapore National Research Foundation (NRF) through the Singapore-MIT Alliance for Research and Technology (SMART), Center for Environmental Sensing and Modeling (CENSAM). The authors also thank the Department of Civil and Environmental Engineering, National University of Singapore for providing computational resources.

NHESSD
1, 2831–2857, 2013

References

Batchelor, G. K.: An Introduction to Fluid Dynamics, Cambridge University Press, UK, 1967.

Bonet, J. and Kulasegaram, S.: Correction and stabilization of smooth particle hydrodynamics methods with applications in metal forming simulations, Int. J. Numer. Meth. Eng., 47, 1189–1214, 2000.

Chan, E. S.: Mechanics of deep water plunging-wave impacts on vertical structures, Coast. Eng., 22, 115–133, 1994.

Chan, E. S. and Melville, W. K.: Deep-water plunging wave pressures on a vertical plane wall, P. Roy. Soc. Lond. A Mat., 417, 95–131, 1988.

Chan, E. S., Cheong, H. F., and Gin, K. Y. H.: Breaking-wave loads on vertical walls suspended above mean sea level, J. Waterway Div.-ASCE, 121, 195–202, 1995.

Colagrossi, A. and Landrini, M.: Numerical simulation of interfacial flows by smoothed particle hydrodynamics, J. Comput. Phys., 191, 448–475, 2003.

Dalrymple, R. A. and Rogers, B. D.: Numerical modeling of water waves with the SPH method, Coast. Eng., 53, 141–147, 2006.

Dao, M. H.: Numerical Study of Plunging Wave in Deep Water, Ph. D. thesis, Civil Engineering, National University of Singapore, Singapore, 2010.

Dao, M. H. and Tkalich, P.: Tsunami propagation modelling – a sensitivity study, Nat. Hazards Earth Syst. Sci., 7, 741–754, doi:10.5194/nhess-7-741-2007, 2007.

Dao, M. H., Tkalich, P., and Chan, E. S.: Tsunami forecasting using proper orthogonal decomposition method, J. Geophys. Res., 113, C06019, doi:10.1029/2007JC004583, 2008.

Dao, M. H., Xu, H., Chan, E. S., and Tkalich, P.: Numerical modelling of extreme waves by Smoothed Particle Hydrodynamics, Nat. Hazards Earth Syst. Sci., 11, 419–429, doi:10.5194/nhess-11-419-2011, 2011.

Dommermuth, D. G, Yue, D. K. P., Lin, W. M., Rapp, R. J., Chan, E. S., and Melville, W. K.: Deep water plunging breakers a comparison between potential theory and experiments, J. Fluid. Mech., 189, 423–442, 1988.

Gingold, R. A. and Monaghan, J. J.: Smoothed particle hydrodynamics: theory and application to non-spherical stars, Mon. Not. R. Astron. Soc., 181, 375–389, 1977.

Gomez-Gesteira, M., Cerqueiroa, D., Crespoa, C., and Dalrymple, R. A.: Green water overtopping analyzed with a SPH model, Ocean Eng., 32, 223–238, 2005.

NHESSD
1, 2831–2857, 2013

Goto, C., Ogawa, Y., Shuto, N., and Imamura, F.: Numerical Method of Tsunami Simulation with the Leap-Frog Scheme (IUGG/IOC Time Project), IOC Manual, No. 35, UNESCO, Paris, France, 1997.
Grilli, S. T., Svendsen, I. A., and Subramanya, R.: Breaking criterion and characteristics for solitary waves on slopes, J. Waterway Div.-ASCE, 123, 102–112, 1997.
Hughes, S. A.: Physical Models and Laboratory Techniques in Coastal Engineering, World Scientific, London, UK, 1993.
Khayyer, A., Gotoh, H., and Shao, S. D.: Corrected incompressible SPH method for accurate water-surface tracking in breaking waves, Coast. Eng., 55, 236–250, 2008.
Kim, S. K., Liu, P. L. F., and Liggett, J. A.: Boundary integral-equation solutions for solitary wave generation, propagation and run-up, Coast. Eng., 7, 299–317, 1983.
Li, Y. and Raichlen, F.: Energy balance model for breaking solitary wave runup, J. Waterway Div.-ASCE, 129, 47–59, 2003.
Liu, M. B. and Liu, G. R.: Restoring particle consistency in smoothed particle hydrodynamics, Appl. Numer. Math., 56, 19–36, 2006.
Liu, P. L. F., Cho, Y. S., Briggs, M. J., Kanoglu, U., and Synolakis, C. E.: Runup of solitary waves on a circular island, J. Fluid Mech., 302, 259–285, 1995.
Lucy, L. B.: Numerical approach to testing the fission hypothesis, Astron. J., 82, 1013–1024, 1977.
Lugni, C., Brocchini, M., and Faltinsen, O. M.: Wave impact loads: the role of the flip-through, Phys. Fluids, 18, 17 pp., doi:10.1063/1.2399077, 2006.
Maiti, S. and Sen, D.: Computation of solitary waves during propagation and runup on a slope, Ocean Eng., 26, 1063–1083, 1999. Mimura, N., Yasuhara, K., Kawagoe, S., Yokoki, H., and Kazama, S.: Damage from the Great East Japan Earthquake and Tsunami – A quick report, Mitigation and Adaptation Strategies for Global Change, 16, 803–818, doi:10.1007/s11027-011-9297-7, 2011.
Oger, G., Doring, M., Alessandrini, B., and Ferrant, P.: An improved SPH method: towards higher order convergence, J. Comput. Phys., 225, 1472–1492, 2007.
Shuto, N. and Goto, C.: Numerical simulations of the transoceanic propagation of tsunamis, in: Sixth Congress Asian and Pacific Regional Division, 20–22 July 1988, International Association for Hydraulic Research, Kyoto, Japan, 1988.
Shuto, N., Goto, C., and Imamura, F.: Numerical simulation as a means of warning for near-field tsunami, Coast. Eng. Jpn., 33, 173–193, 1990.

NHESSD
1, 2831–2857, 2013

Titov, V. V. and Synolakis, C. E.: Numerical modeling of tidal wave runup, J. Waterway Div.-ASCE, 124, 157–171, 1998.
Tkalich, P. and Dao, M. H.: Tsunami modelling and forecasting techniques environmental hazards, in: The Fluid Dynamics and Geophysics of Extreme Events, edited by: Moffatt, K. and Shuckburgh, E., Lecture Notes Series, Institute for Mathematical Sciences, National University of Singapore, 21, World Scientific, ISBN:978–981-4313-28-5, 269–294, 2011.
US Geological Survey: Magnitude 9.0 – near the east coast of Honshu, Japan, available at: http://earthquake.usgs.gov/earthquakes/eqinthenews/2011/usc0001xgp/usc0001xgp.php, last accessed: 04 December 2012, last modified: 27 October 2012.
Vidal, Y., Bonet, J., and Huerta, A.: Stabilized updated Lagrangian corrected SPH for explicit dynamic problems, Int. J. Numer. Meth. Eng., 69, 2687–2710, 2007.
Ward, D. L.: Physical Model Study of Revere Beach, Massachusetts, US Army Engineer Waterways Experiment Station, Vicksburg, Miss., USA, 71 pp., 1995.
Xu, H.: Numercial Simulation of Breaking Wave Impact on Structures, Ph. D. thesis, Civil Engineering, National University of Singapore, Singapore, in press, 2013.
Xu, H., Dao, M. H., and Chan, E. S.: An SPH model with C1 consistency, in: 5th Internetional SPHERIC Workshop, edited by: Rogers, B. D., Manchester, 2010.
Yalciner, A., Pelinovsky, E., Talipova, T., Kurkin, A., Kozelkov, A., and Zaitsev, A.: Tsunamis in the Black Sea: comparison of the historical, instrumental, and numerical data, J. Geophys. Res., 109, C12023, doi:10.1029/2003JC002113, 2004.

NHESSD
1, 2831–2857, 2013

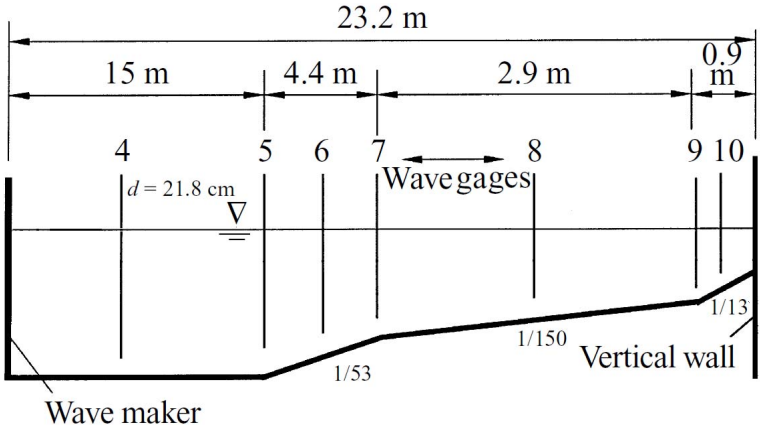

Fig. 1. Experiment setup.

NHESSD
1, 2831–2857, 2013

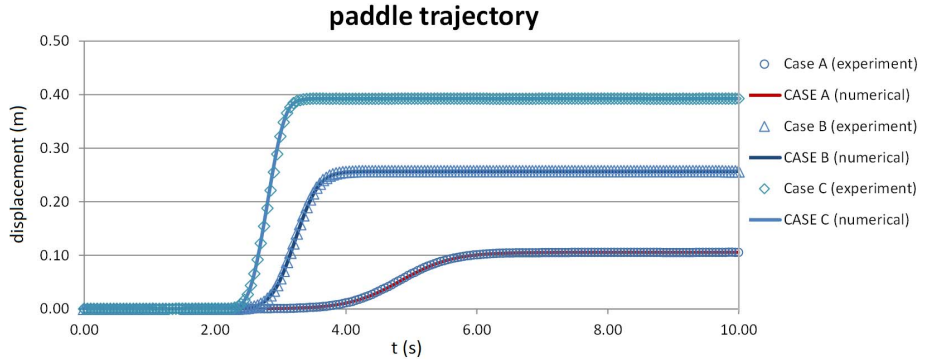

Fig. 2. Paddle trajectory used experiments and numerical simulations of three cases of solitary waves.

NHESSD
1, 2831–2857, 2013

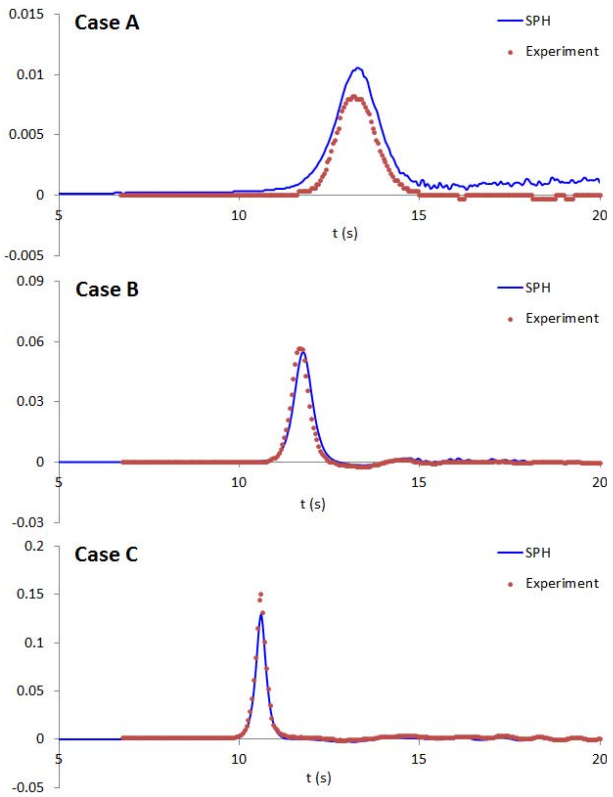

Fig. 3. Water levels recorded at gage 4.

NHESSD
1, 2831–2857, 2013

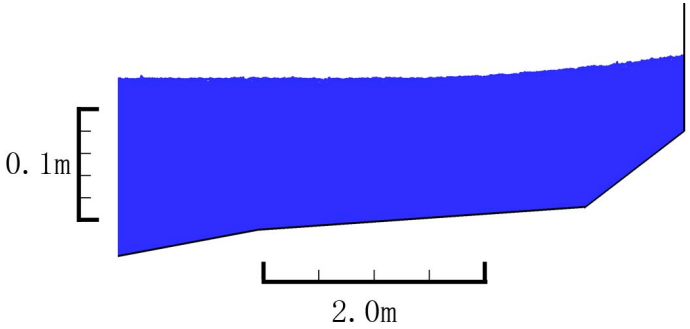

Fig. 4. Snapshot of solitary wave impact on the wall in Case A (obtained from the SPH simulation).

NHESSD
1, 2831–2857, 2013

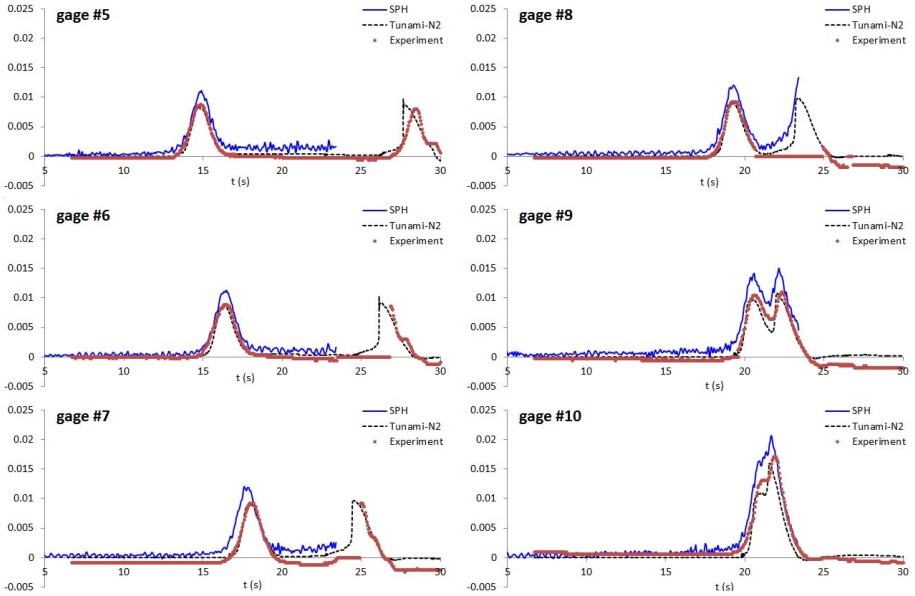

Fig. 5. Comparisons of time histories of wave height obtained from the experiment and numerical simulations at gage 5 to gage 10 of Case A.

NHESSD
1, 2831–2857, 2013

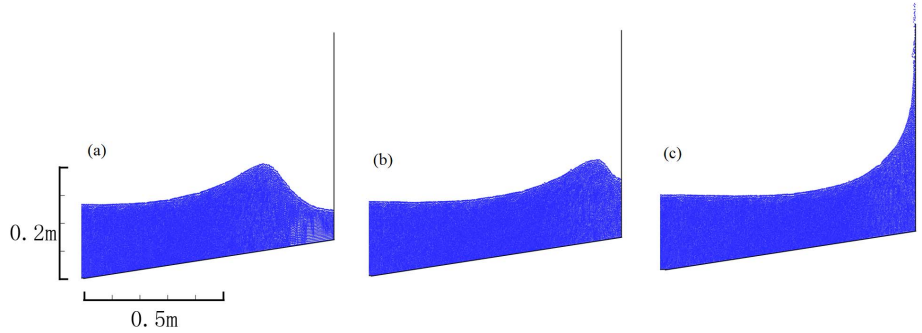

Fig. 6. Snapshots of wave approaching and impacting on the wall for Case B (obtained from the SPH simulation).

NHESSD
1, 2831–2857, 2013

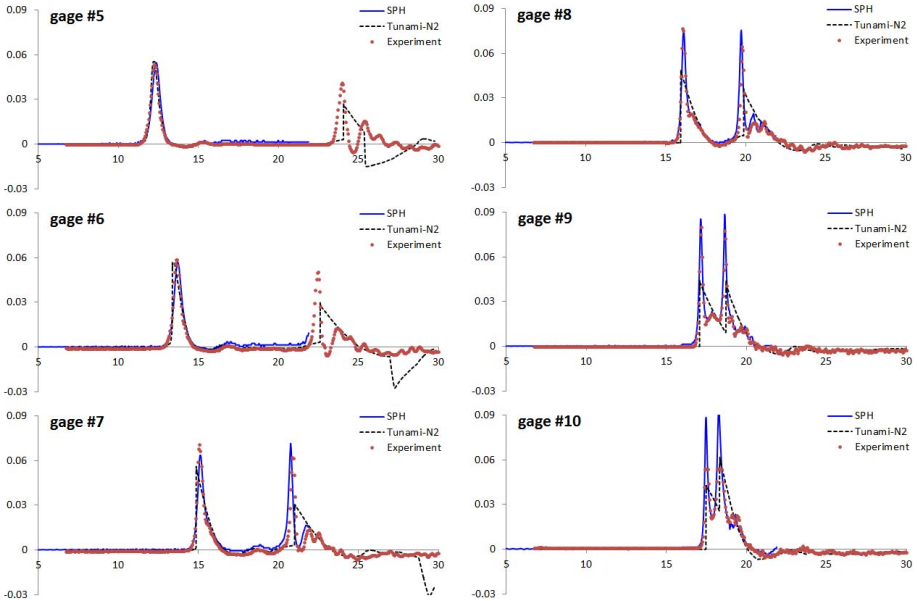

Fig. 7. Comparisons of time histories of wave height obtained from the experiment and numerical simulations at gage 5 to gage 10 of Case B.

NHESSD
1, 2831–2857, 2013

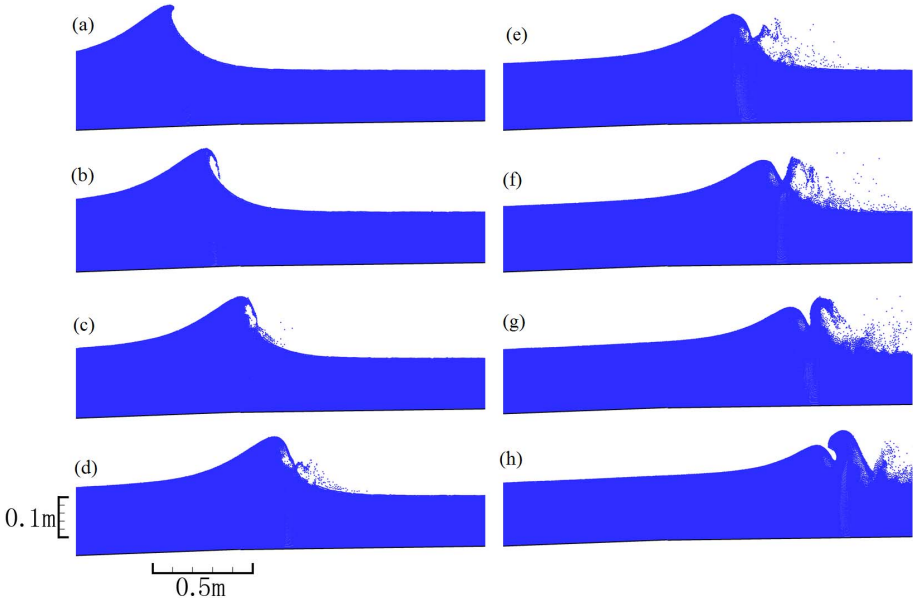

Fig. 8. Snapshots of wave breaking in Case C (obtained from the SPH simulation).

NHESSD
1, 2831–2857, 2013

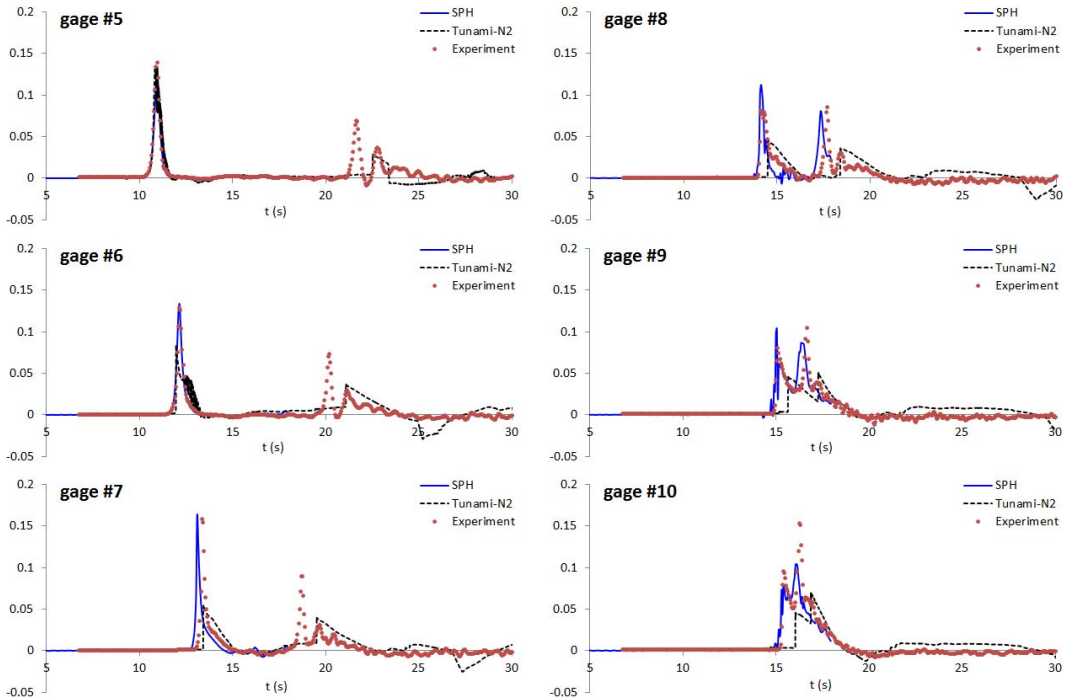

Fig. 9. Comparisons of time histories of wave height obtained from the experiment and numerical simulations at gage 5 to gage 10 of Case C.

NHESSD
1, 2831–2857, 2013

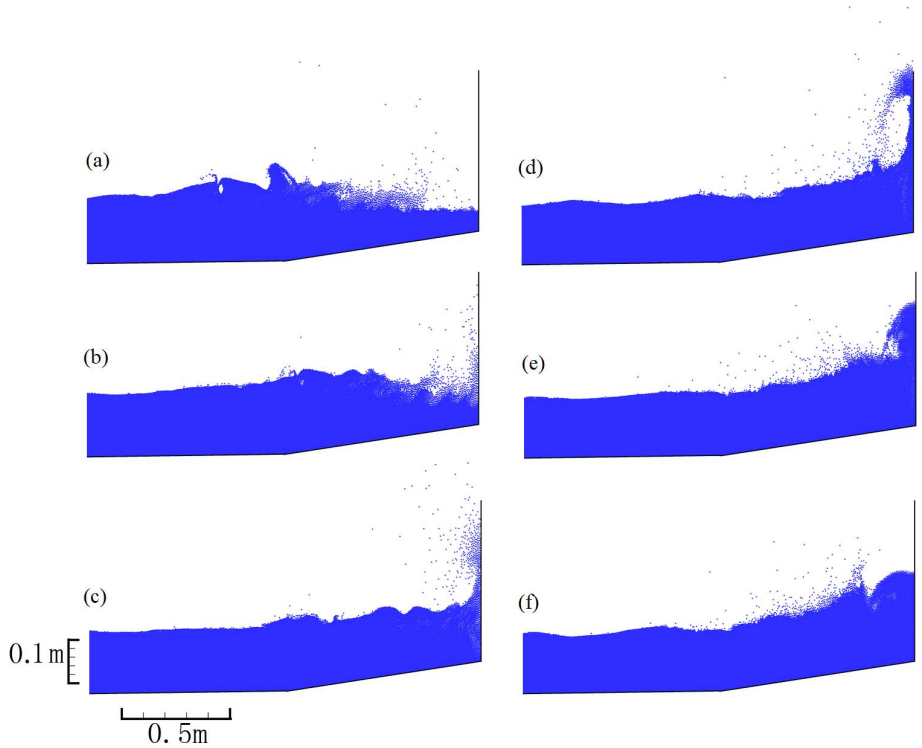

Fig. 10. Snapshots of breaking wave impact on the wall for Case C (obtained from the SPH simulation).

NHESSD
1, 2831–2857, 2013

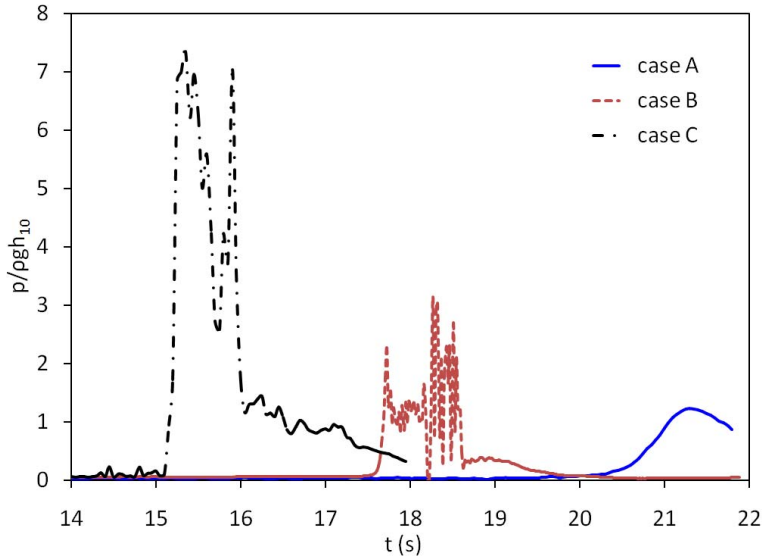

Fig. 11. Pressure time histories due to wave impact on the wall (obtained from the SPH simulations).

NHESSD
1, 2831–2857, 2013